Chapter 2
Theoretical Modeling of Aeroheating Under Rarefied Gas Effects

In the Chap. 1, it has been mentioned that the utmost critical points concerning thermal protection are the stagnation point of the leading edge and the reattachment point behind a separation flow region. The wall surfaces near these points suffer from peak heat fluxes, and thus the surface temperature is relatively higher than elsewhere. These most dangerous regions are likely to be ablated first, and should be specially protected by UHTC materials. Therefore, our target is currently focused on the prediction of aeroheating performance of the typical stagnation point region, although the methodology and some conclusions are universal to an extent. In fact, we have found that the engineering theory established at the stagnation point region is also useful for analogy analysis of other regions.

In this chapter, nonlinear factors in the flow and heat transfer are regarded as the macroscopic behavior of rarefied gas effects resulting from the microscopic non-equilibrium collisions of molecules. We first propose a simplified physical model and a corresponding mathematical description of the stagnation point flow in the near-continuum regime. Then after an approximately analytical treatment, we obtain some quantitative and theoretical results. Finally, based on comparisons with DSMC results and experimental data, we find that these results could be extended to more rarefied flow regimes, leading to a qualitatively correct and quantitatively rational engineering theory.

2.1 Problem Description

Generally, the sharpened nose and wingtip of a near-space hypersonic cruise vehicle can be modeled, respectively, as a slightly spherically blunted cone and a cylindrically blunted wedge, as shown in Fig. 2.1, where θ represents the half angle of the cone or wedge and M_∞ the hypersonic free stream Mach number. For a given free stream condition, a smaller and smaller R_N indicates a more and more rarefied flow. As R_N decrease continuously toward 0, the flow will approach the free molecular flow limit.

© Springer-Verlag Berlin Heidelberg 2015

Z.-H. Wang, *Theoretical Modelling of Aeroheating on Sharpened Noses Under Rarefied Gas Effects and Nonequilibrium Real Gas Effects*, Springer Theses,
DOI 10.1007/978-3-662-44365-1_2

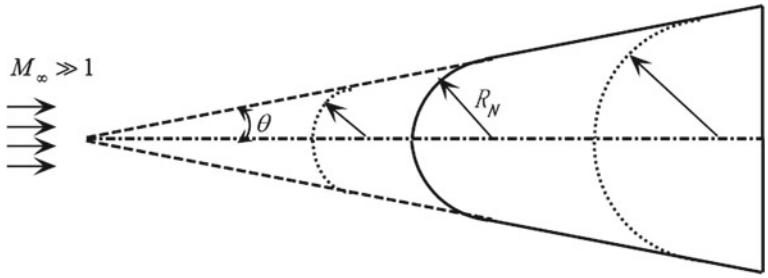


Fig. 2.1 Schematic diagram of a sharp leading edge

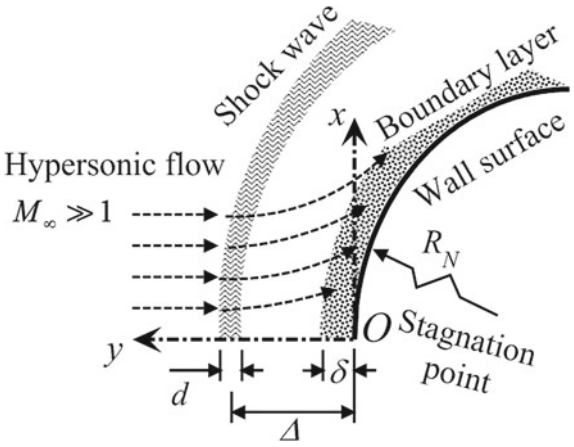


Fig. 2.2 Typical hypersonic flow field around a nose

A specific aeroheating prediction theory corresponds to a flow field structure pattern. Before producing an aeroheating prediction theory of sharp leading edges, we need to gain a clear understanding of the flow field feature near the stagnation point. Figure 2.2 demonstrates a typical stagnation point flow field (only half is given due to symmetry), with d, δ and Δ being the shock wave thickness, SPBL thickness and the stand-off distance of the bow shock wave, respectively.

For a high Reynolds number continuous flow, $\Delta \gg \delta$ and $\Delta \gg d$, i.e., both the shock wave and the boundary layer are very thin, and the flow field is characterized by a triple layer structure. The viscous effects are restricted to thin layers of the shock wave and the boundary layer, and the flow between them could be considered as inviscid.

The Fay–Riddell equation [1] was introduced based exactly on this flow field structure, and a typical version for prediction of the SPBL heat transfer of an axisymmetric nose takes the form of

$$q_s = 0.763 Pr^{-0.6} (\rho\mu)_w^{0.1} (\rho\mu)_s^{0.4} \beta_s^{0.5} \left[1 + \left(Le_f^n - 1\right) \frac{h_D}{h_s}\right] (h_s - h_w) \quad (2.1)$$

where the subscripts s and w indicate the stagnation point and wall surface conditions, respectively; Pr and Le are the Prandtl number and Lewis number, respectively; and ρ represents gas density, μ the viscosity, β the tangential velocity gradient at the outer edge of SPBL, h the enthalpy and h_D the dissociation enthalpy at the outer edge of the SPBL. For a two-dimensional leading edge case, the constant coefficient on the right-hand side of Eq. 2.1 should be 0.57. The power exponent of Lewis number takes the value of 0.52 for an equilibrium boundary layer, and 0.63 for the case with a frozen boundary layer and a fully catalytic wall surface. Since the Lewis number is approximate to 1, the real gas effects is insignificant, and the predictions with $n = 0.52$ and 0.63 are almost identical. However, for the non-catalytic wall and nonequilibrium boundary layer cases, the conclusion will be different, as will be detailed in the fourth chapter.

Equation 2.1 shows that the heat flux to the wall surface is mainly determined by the flow state at the outer edge of the SPBL, and this state needs to be calculated on the basis of the post-shock inviscid flow. Therefore, the existence of an inviscid external flow field is a precondition of the Fay–Riddell equation. For hypersonic flows, the tangential velocity gradient at the outer edge of the SPBL could be obtained from the modified Newton equation [2],

$$\beta_s \approx \frac{1}{R_N} \sqrt{\frac{2(p_s - p_\infty)}{\rho_s}} \approx \frac{1}{R_N} \sqrt{\frac{2p_s}{\rho_s}} = \sqrt{\frac{2}{\gamma}} \frac{a_s}{R_N} \quad (2.2)$$

where $p = \rho RT$ represents the pressure, and $p_s \gg p_\infty$ in hypersonic flows; $a = \sqrt{\gamma RT}$ represents the speed of sound, with R and γ being the gas constant and the equivalent specific heat ratio.

Substituting Eq. 2.2 into Eq. 2.1, we observe that the stagnation point heat flux is in inverse proportion to the square root of the radius of curvature of the leading edge, i.e., $q_s \propto 1/\sqrt{R_N}$. This is the main characteristic of aeroheating in the continuous flow regime. The Fay–Riddell equation will predict an infinite q_s if R_N continuously decreases to 0. Of course, it is physically impossible in practice. But we are curious about what will happen in this process and how the actual aeroheating performance will evolve. Let us first have an analysis of the evolution of the flow field structure.

With R_N decreasing continuously, the flow will become rarefied, and the flow field pattern will transform gradually. An expansion of the viscous flow region manifests first, i.e. the shock stand-off distance is small, but the thicknesses of the boundary layer and the shock wave will grow a lot to lead to $\delta + d/2 \sim \Delta$. The growing shock wave and boundary layer will touch, partly overlap, and even merge with each other to cause viscous interaction effects, and then nonequilibrium and nonlinear factors become significant. For these cases where the inviscid flow region disappears, the Fay–Riddell equation fails. If the rarefaction degree increases further, there will be no distinct shock wave or boundary layer observed, effects of the velocity slip and

the temperature jump at the surface will also become important, and the flow will finally approach the free molecular flow limit. There is still no sophisticated theory to describe these phenomena after successive failures of the boundary layer assumption and the continuum hypothesis.

A specific performance of the failure of the Fay–Riddell equation is that the actual stagnation point heat flux is no longer inversely proportional to the square root of the nose radius, but gradually approaches a limit. The questions at present are how the variation of heat flux with the nose radius derives from the original relation, what flow mechanism is involved, and how to give a quantitative description.

2.2 Analysis and Research Idea

According to the above section, we have known that as the flow transits from the continuous to the rarefied state, the flow field structure will undergo a great change, and the corresponding aeroheating performance also changes significantly with it. However, this is a gradual and continuous process without clear boundaries, and the thickening, touching, and interaction of the shock wave and boundary layer also occur successively. The gradual failure of NSF equations under the continuum hypothesis, as well as that of the Fay–Riddell equation based on further boundary layer assumption, must be accompanied by an increasingly significant factor that results in their invalidations. This factor is one of those that are ignored in NSF equations, but should be regained and specially considered at present. In order to figure out what factor is becoming significant to result in the failure of NSF equations, we need to adopt a more advanced equation system which is valid in both the continuum and rarefied flow regime.

Accordingly, in the present theoretical modeling study, we turn our attention to Burnett equations that are of higher order than NSF equations, and propose a physical model in the near-continuum regime to carry on the analysis. It is found that the rarefied gas effects resulting from microscopic insufficient collisions of molecules manifest as an increase in the nonlinear effects in macroscopic flow and heat transfer. Therefore, we emphatically analyze the failure of the linear Fourier law and the enhancing effect of the nonlinear non-Fourier heat flux. Additionally, we also employ the DSMC method which also applies to both rarefied and continuous flows to carry out supporting calculations. Finally, after systematic validations, results from the theoretical modeling study are extended to form an engineering theory.

2.3 Nonlinear Heat Transfer in Hypersonic Rarefied Flows

2.3.1 Theoretical Basis

Basically, the transfers of mass, momentum, and energy in fluid are implemented by the random movements and collisions of molecules, and these processes can be described by Boltzmann equation [3]. For a simple dilute gas, its expression is

$$\frac{\partial f}{\partial t} + c \cdot \frac{\partial f}{\partial \mathbf{r}} + F \cdot \frac{\partial f}{\partial c} = \int_{-\infty}^{\infty} \int_{0}^{4\pi} \left(f^* f_1^* - f f_1 \right) c_r \sigma \, \mathrm{d}\Omega \, \mathrm{d}c_1 \tag{2.3}$$

in which $f(t, c, r)$ is the molecular velocity distribution function, t the time variable, $r = (x, y, z)$ the position vector, $c = (u, v, w)$ the velocity vector, F the external force per unit mass, c_r the relative velocity, σ the collision cross section, Ω the solid angle, and the superscript * indicates an inverse collision. The righthand side of Eq. 2.3 is called the collision term, representing the rate of increase of molecules of class c in the phase space element $\mathrm{d}c\mathrm{d}r$ as a result of the combined direct and inverse collisions. For a gas mixture, collisions between molecules of different species must also be considered separately.

Boltzmann equation is a complex multiple integral-differential equation whose direct solution is extremely vexatious, if not impossible. Consequently, we have to resort to its Chapman-Enskog asymptotic expansion [3] in the neighborhood of the flow state with equilibrium collisions, and obtain some approximate equations under various conditions. The expansion of the velocity distribution function is

$$f = f^{(0)} + f^{(1)} + f^{(2)} + \cdots \tag{2.4}$$

And then, the corresponding series expansion of heat flux is

$$q = q^{(0)} + q^{(1)} + q^{(2)} + \cdots \tag{2.5}$$

where $q^{(n)} = \int E c f^{(n)} \mathrm{d}c$ with E as the molecular energy. The zeroth order approximation produces Euler equations with the corresponding heat flux $q^{(0)} = 0$, and the first order approximation produces Navier–Stokes equations and the Fourier law $q^{(1)} = -K \nabla T$ with K as the heat conductivity. Successively, the second order approximation leads to the Burnett equations whose heat flux is $q^{(1)} + q^{(2)}$ and $q^{(2)}$ could be written in the tensor form as

$$\begin{aligned} q_i^{(2)} = {} & \theta_1 \frac{\mu^2}{\rho T} \frac{\partial u_j}{\partial x_j} \frac{\partial T}{\partial x_i} + \theta_2 \frac{\mu^2}{\rho T} \left[-\frac{2}{3} \frac{\partial}{\partial x_i} \left(T \frac{\partial u_j}{\partial x_j} \right) - 2 \frac{\partial u_j}{\partial x_i} \frac{\partial T}{\partial x_j} \right] \\ & + \left[\theta_3 \frac{\mu^2}{\rho p} \frac{\partial p}{\partial x_j} + \theta_4 \frac{\mu^2}{\rho} \frac{\partial}{\partial x_j} + \theta_5 \frac{3\mu^2}{\rho T} \frac{\partial T}{\partial x_j} \right] \left[\frac{1}{2} \left(\frac{\partial u_j}{\partial x_i} + \frac{\partial u_i}{\partial x_j} \right) - \frac{1}{3} \frac{\partial u_k}{\partial x_k} \delta_{ij} \right] \end{aligned} \tag{2.6}$$

where δ_{ij} is Kronecker-delta function which equals 1 if $i = j$, or 0 if $i \neq j$; θ_1 to θ_5 are constants in relation to the molecular model, and if the hard sphere model [3] is employed, $\theta_1 = 11.644$, $\theta_2 = 5.822$, $\theta_3 = -3.090$, $\theta_4 = 2.418$ and $\theta_5 = 25.157$.

$q^{(2)}$ and the terms after it represent the high order nonlinear factors in the flow and heat transfer. In the continuous flow regime, the high order nonlinear heat flux is negligible compared to $q^{(1)}$. But when the flow becomes rarefied, the influence of the nonlinear heat flux will increase and even exceed that of the linear heat flux.

Seemingly, Burnett approximation is more suitable to be used to solve the rarefied flow problems. However, due to its complexity, it is almost impossible to use it in a theoretical study. Its application in the numerical simulation also suffers from various complications, and the results calculated are not much better than those from the NSF-based CFD. Even the stability of its solution is still in debate and needs further investigations. All these factors restrict the direct application of Burnett equations and the higher order approximations to very limited problems.

But this does not mean that Burnett approximation is completely useless. An analysis of the nonlinear terms in its transport equation will help us to judge how far NSF equations deviate from a competent description. Since the nonlinear feature is mainly characterized by the product terms of the flow field gradients, its relative impact is significant only in regions with large gradients, such as those near the shock wave or close to the wall surface. Just in these regions, the local Knudsen number Kn_{local} is relatively larger than elsewhere, indicating that the rarefied gas effects first appeared or are relatively more significant, as shown in Fig. 2.3. Therefore, similar to Kn_{local} , the ratio of the nonlinear non-Fourier heat flux terms to the linear terms should also be capable of predicting the rarefaction degree of the local flow field.

In fact, as early as 1946, Tisen [4] made a qualitative order of magnitude estimate of the ratio of the second to first order terms of Burnett equations, and concluded that Burnett equations should be more suitable than NSF equations in solving the slightly rarefied hypersonic flow with velocity slip. Recently, Lockerby, Reese and Struchtrup [5] introduced a type of switching criteria for hybrid rarefied gas flow solvers by considering the relative error between the flow fields calculated by an NSF

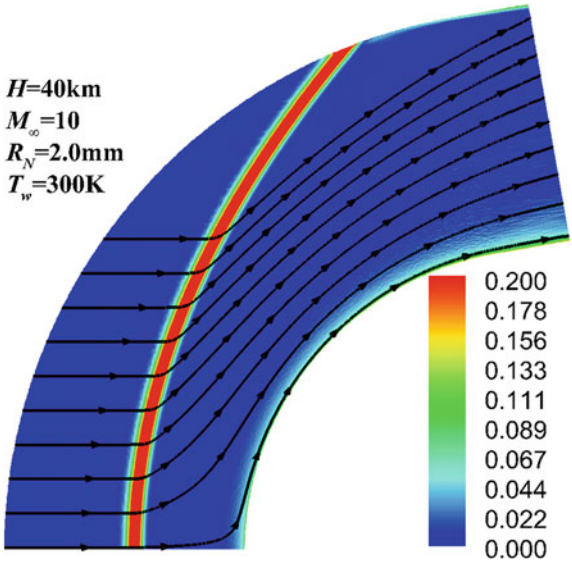


Fig. 2.3 A DSMC result of local Knudsen number contour of a 2.0 mm radius nose flying with a Mach number 10 at 40 Km altitude

solver and a molecular/kinetic or higher order continuum solver. It is worth noting that, although in the introduced parameters the form of the shear stress and heat flux of Burnett equations are adopted, the involved physical quantities actually come from the flow field calculated by the NSF-based CFD method or DSMC method, rather than from that directly computed by Burnett equations. However, their results suggest that this technique is not only feasible, but also physically reasonable, because of the fact that in the near-continuum regime, when considering only the macroscopic flow quantities, for instance temperature and density, there is not much difference among predictions of NSF equations, Burnett equations, and DSMC method, and the discrepancy first appears in the higher order gradients of the flow field. With evident physical meanings, these criteria introduced by Lockerby seem the most useful and robust among the "local Knudsen number" like parameters. But these criteria could only be used in numerical simulations, because it is impossible to foresee the flow field information in practice. It will be meaningful if we can theoretically study the ratio of the non-Fourier to the Fourier part of the heat flux terms in Burnett equations to obtain an analytical criterion of rarefied flows. Particularly, this criterion is directly related to the heat transfer calculation and could be used to predict the aeroheating performance of rarefied flows.

Actually, almost simultaneously with Lockerby's work but independently, we adopted a somewhat similar idea in our theoretical modeling study to get a rarefaction criterion, which is of physical significance and universal for aeroheating in hypersonic rarefied flows.

2.3.2 Rarefied Flow Criterion

To take into account the nonlinear factors in rarefied flows, we attempt to design a heat flux expression as follows in the stagnation point region:

$$q_s = q_{\mathrm{F}} + q_{\mathrm{NF}} \tag{2.7}$$

with q_{F} still being the Fourier heat flux and q_{NF} denoting the nonlinear correction from the non-Fourier heat flux. But instead of directly using Eq. 2.6, we intend in advance to analyze each of the nonlinear terms to figure out the most important factors and to get a concise but practical result.

First, as only the flow field near the stagnation streamline is concerned, the flow quantities p, ρ, T, and v are symmetrical about the stagnation streamline (y-coordinate), while u is anti-symmetrical, as shown in Fig. 2.2. Therefore, in the neighborhood of the stagnation point,

$$\begin{cases} p = p_0(y) + p_{xx}(y)x^2/2 + \cdots \\ \rho = \rho_0(y) + \rho_{xx}(y)x^2/2 + \cdots \\ T = T_0(y) + T_{xx}(y)x^2/2 + \cdots \\ v = v_0(y) + v_{xx}(y)x^2/2 + \cdots \\ u = u_x(y)x + \cdots \end{cases} \tag{2.8}$$

Substituting Eq. 2.8 into Eq. 2.6 leads to the first simplification, and when high order terms are truncated, we get

$$q_y^{(2)} = \frac{\mu^2}{\rho T}\left[\alpha_1 \frac{\partial v}{\partial y}\frac{\partial T}{\partial y} + 2^J \alpha_2 \frac{\partial u}{\partial x}\frac{\partial T}{\partial y} + \alpha_3 T \frac{\partial^2 v}{\partial y^2} + 2^J \alpha_4 T \frac{\partial^2 u}{\partial x \partial y}\right] \tag{2.9}$$

where $J = 0$ or 1 corresponds to a two-dimensional or axisymmetric leading edge model, respectively; the constants $\alpha_1 = \theta_1 - 8\theta_2/3 + 2\theta_5 \approx 46.433$, $\alpha_2 = \theta_1 - 2\theta_2/3 - \theta_5 \approx -17.394$, $\alpha_3 = 2(\theta_4 - \theta_2)/3 \approx -2.269$, and $\alpha_4 = (\theta_4 - 4\theta_2)/6 \approx -3.478$. In the deduction, we have used the equation of state and the conclusion that pressure is approximate to a constant across the SPBL, i.e., $\partial p/\partial y \approx 0$.

Equation 2.9 is still so complex that further simplifications are needed to catch the most important factor. The general solutions [6] of the hypersonic laminar boundary layer suggests the following relations near the stagnation point:

$$\begin{cases} \dfrac{\partial v}{\partial y} = -2^J \beta_s \\ \dfrac{\partial u}{\partial x} = -\dfrac{1}{2^J \rho}\dfrac{\partial (\rho v)}{\partial y} = \dfrac{\rho_s}{\rho}\beta_s \end{cases} \tag{2.10}$$

Since β_s is a constant, and inside the SPBL $p = \rho RT$ is approximate to a constant, we get $\partial u/\partial x \approx T\beta_s/T_s$, $\partial^2 v/\partial x^2 \approx 0$ and $\partial^2 u/\partial x \partial y \approx (\beta_s/T_s)\partial T/\partial y$. Thus, Eq. 2.9 becomes

$$q_y^{(2)} = -2^J \left[\alpha_1 - (\alpha_2 + \alpha_4)\frac{T}{T_s}\right]\sqrt{\frac{2}{\gamma}}\frac{a_s}{R_N}\frac{\mu^2}{\rho T}\frac{\partial T}{\partial y} \tag{2.11}$$

Equation 2.11 gives a specific expression of q_{NF} in Eq. 2.7, and it could be used to bring in a first order correction in calculating the heat flux in practice. However, this is not the point we are most interested in, and we want to theoretically estimate the relative impact of this heat flux correction. Therefore, we further definite the ratio of the non-Fourier to Fourier heat flux terms as a flow parameter W, and then find its characteristic value W_r inside the SPBL, namely

$$W_r = \frac{q_{\mathrm{NF}}}{q_{\mathrm{F}}} \approx 2^J \alpha_1 \left(1 + 0.45\frac{T_r}{T_s}\right)\sqrt{\frac{2}{\gamma}}\frac{a_s}{R_N}\left(\frac{\mu^2}{\rho T K}\right)_r \tag{2.12}$$

where the subscript r indicates that the quantities should be calculated based on the corresponding reference enthalpy which is chosen as the average value of the enthalpy at the external edge of the SPBL and the wall surface enthalpy. When the high temperature real gas effects are not much significant, it is appropriate to approximately calculate them at the mean temperature inside the boundary layer, i.e., $T_r = (T_s + T_w)/2$. For diatomic gases [3], $K = (9\gamma - 5)\mu R/[4(\gamma - 1)]$, $\mu \propto T^{\omega}$ with ω being the viscosity-temperature index. Then, Eq. 2.12 could be

simplified to

$$W_r \approx 2^J \alpha_1 \frac{4\sqrt{2\gamma}\,(\gamma-1)}{(9\gamma-5)} \left(1.225 + 0.225\frac{T_w}{T_s}\right) \left(\frac{T_s+T_w}{2T_s}\right)^{\omega} \frac{\mu_s}{\rho_s a_s R_N} \tag{2.13}$$

Furthermore, in hypersonic flows, $\rho_s/\rho_\infty \approx (\gamma+1)/(\gamma-1)$, $T_s/T_\infty \approx (\gamma-1)M_\infty^2/2$, and then,

$$W_r \approx 2^J \frac{M_\infty^{2\omega}}{Re_\infty} \frac{4.9\alpha_1\sqrt{2\gamma}(\gamma-1)^{\omega+3/2}}{2^{2\omega}\,(\gamma+1)\,(9\gamma-5)} \left(1 + 0.184\frac{T_w}{T_s}\right) \left(1+\frac{T_w}{T_s}\right)^{\omega} \tag{2.14}$$

where, $Re_\infty = \rho_\infty V_\infty R_N/\mu_\infty$ is the free stream Reynolds number. For most practical hypersonic air flows, $\omega \approx 0.75$, and T_w is much lower than T_s. Thus, to be concise and direct, a final first order approximation about T_w/T_s yields

$$W_r \approx 2^J \frac{M_\infty^{3/2}}{Re_\infty} \Gamma(\gamma) \left(1+\frac{T_w}{T_s}\right) \tag{2.15}$$

in which $\Gamma(\gamma) \approx 114\gamma^{1/2}\,(\gamma-1)^{9/4}/(\gamma+1)\,(9\gamma-5)$, and $0.94 > \Gamma > 0.56$ as $1.4 > \gamma > 1.3$. In Eq. 2.15, T_s rather than a function of T_∞ is used, because in most hypersonic experiments, the stagnation temperature T_s , or approximately saying the total temperature, can be obtained more easily than T_∞.

For highly cooled wall cases ($T_w/T_s \ll 1$) with insignificant real gas effects, we will get the most concise version

$$W_r \approx 2^J \frac{M_\infty^{3/2}}{Re_\infty} \tag{2.16}$$

By this means, we find a characteristic flow parameter that depends completely on the free stream conditions. W_r quantitatively represents the influence of nonlinear factors relative to the linear Fouriers law in the SPBL heat transfer, indicating the failure of the continuous NSF equations, and thus could be considered as a criterion of the rarefied gas effects.

It could be easily observed that the criterion W_r is different in form from the free stream Knudsen number $Kn_\infty = \lambda_\infty/R_N$, and in fact, $W_r \approx 2^J(2M_\infty/\pi\gamma_\infty)^{1/2}$ Kn_∞. As stated by Macrossan [7], being a ratio of two characteristic lengths, Kn_∞ is only a state parameter rather than a flow parameter, and cannot sufficiently describe hypersonic flows, especially those involving the aeroheating problem. We have found that W_r is approximately inversely proportional to the modified Cheng's parameter K_Λ^2, a fitted correlation parameter that is popularly used in the engineering practice. This parameter was first introduced by Cheng [8] based on the TVSL model, and later modified by Engel [9] according to correlation with the experimental data. Its expression is

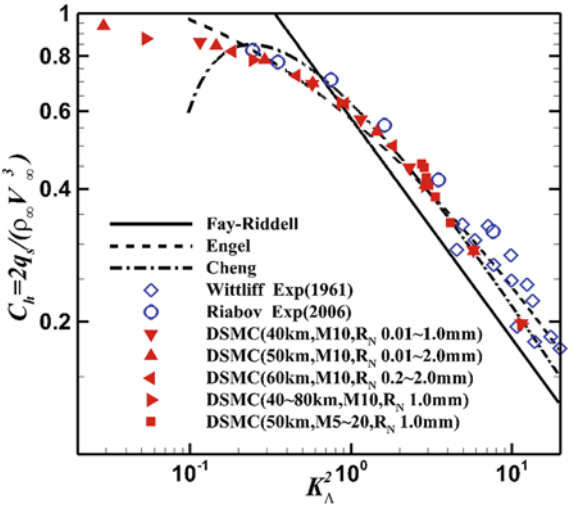


Fig. 2.4 The stagnation point heat transfer coefficients for slightly blunted cones varies with modified Cheng's parameter

$$K_\Lambda^2 = \frac{\gamma_\infty - 1}{2\gamma_\infty} Z_e Re_\infty \frac{\mu_\infty T_r}{\mu_r T_s} \approx \frac{Z_e Re_\infty}{\gamma_\infty M_\infty^2} \frac{\mu_\infty T_r}{\mu_r T_\infty} \tag{2.17}$$

where Z_e is the compressibility factor, and approximately equals 1 if the real gas effects are insignificant. After simplification and comparison, it is shown $W_r \propto 1/K_\Lambda^2$. In the engineering practice, K_Λ^2 has been widely used to normalize and to compare various experimental and numerical data [10–14], and fitted formulas based on K_Λ^2 have extended the scope of application to flows in the near free molecular flow regime. Figure 2.4 demonstrates the variation trend of the stagnation point heat transfer coefficients of spherically blunted cones with different nose radii under various incoming free stream conditions. After being normalized by K_Λ^2, the experimental data [9, 15, 16], the present DSMC results and two typical fitted formulas basically fall on the same curve.

Therefore, according to the explicit relationship between the present W_r and K_Λ^2, the physical meanings of W_r could also be qualitatively extended to more rarefied flow regimes, although it is derived in the near-continuum flow regime. It could be assuredly concluded that W_r is a reliable rarefaction criterion in the whole flow regime. Particularly in the near continuum flow regime, it quantitatively measures the relative impact of the non-Fourier terms in calculation of the stagnation point heat flux.

In the following, we show that W_r has more universal physical meanings. It covers the influence of the nose shape and wall temperature, and could be used to study the aeroheating performance of various models in a normalized way, including the two-dimensional and axisymmetric noses, the highly cooled wall and those not so cold. It could also be used to predict the evolution of the flow field structure as the degree

of rarefaction varies, and thus provides a physical basis to classify the flow regime and design bridging functions for prediction of the aeroheating performance in each regime. Meanwhile, the heat flux distribution along the surface downstream of the stagnation point region can also be approximately estimated based on W_r. Even more, some parameters with a similar expression to W_r have been applied to analysis of the aerodynamic force-related problems [17].

In order to make a physically meaningful flow regime classification, we need not only to find a good criterion, but also to determine the boundaries of each regime by analyzing the flow mechanism to avoid arbitrariness, which leads to the content of the next subsection.

2.3.3 Analysis of Flow Field Structure Features

As mentioned above, a specific aeroheating prediction method should be based on a clear understanding of the corresponding flow field structure. In rarefied flow regime, in the flow field structure shown in Fig. 2.2 there will emerge a gradual and successive evolution as the rarefaction degree increases. The boundary layer and the shock wave will thicken and go closer to each other, leading to touch, overlap, and even mergence. This interaction process is precisely accompanied by the enhancement of the nonlinear effects in the flow and heat transfer. In many early studies, the variation of the aeroheating performance was directly considered to be caused by viscous interaction between the shock wave and the boundary layer. Of course, this NSF-based viewpoint has some truth to it, and currently, it is still a comparatively effective method to deal with the slightly rarefied flows. But from a broader point of view, both the evolutions of the flow field structure and the aeroheating performance arise from the microscopic insufficient collisions of molecules, and are actually two specific manifestations of the rarefied gas effects. Hence, an analysis on the evolution process of the flow field structure and the subsequent exploration on its relation to the rarefaction criterion will be helpful to more deeply and broadly understand the aeroheating performance in the rarefied flow regime and to explain the corresponding physical mechanism.

Therefore, we introduce here a flow field structure parameter Θ in the near-continuum flow regime to indicate the relative size of the viscous region within the shock wave stand-off distance

$$\Theta = \frac{d/2 + \delta}{\Delta} \tag{2.18}$$

It is certain that the feature of the flow field completely depends on the rarefaction degree of the flow. Since W_r has been shown above to measure the rarefaction degree, it will be meaningful to explore the inherent relationship between the parameters Θ and W_r. Therefore, each of the three scales in Eq. 2.18 is discussed one by one as follows.

First, the bow shock wave near the stagnation streamline is equivalent to a normal shock wave, and its thickness is determined by the maximum density gradient across it, i.e.,

$$d = \frac{\rho_2 - \rho_1}{|\partial\rho/\partial y|_{\text{Max}}} \tag{2.19}$$

in which subscripts 1 and 2 denote the condition ahead and behind the shock wave, respectively. Generally speaking, d is only a few times the MFP of molecules. More detailed studies [18, 19] show that the normalized thickness of shock wave d/L^* is Mach number independent in hypersonic flows and approaches about 6.0 for diatomic gases. $L^* = \mu(T^*)/\rho v$ is a kinetic length scale defined under the sonic condition of the flow with the critical temperature $T^* \approx (\gamma - 1)M_\infty^2 T_\infty/(\gamma + 1)$. Referring to $\mu \propto T^\omega$, and $\rho v = \rho_\infty V_\infty$ across the shock wave, it yields $L^*/R_N = (\gamma - 1)^\omega M_\infty^{2\omega}/[(\gamma + 1)^\omega Re_\infty]$. Therefore,

$$\frac{d}{R_N} \approx 6\left(\frac{\gamma - 1}{\gamma + 1}\right)^\omega \frac{M_\infty^{2\omega}}{Re_\infty} \approx \frac{6}{2^J}\left(\frac{\gamma - 1}{\gamma + 1}\right)^\omega \left(1 + \frac{T_w}{T_s}\right)^{-1} W_r \tag{2.20}$$

It is shown that d varies nearly proportionally to W_r.

Secondly, the thickness of the SPBL in hypersonic flows could be similar in form to that in low speed flows on condition that the involved quantities, for instance viscosity and density, take into account the high temperature and compressibility correction. It can be expressed as

$$\delta \approx 2^{(3-J)/2}\frac{x}{\sqrt{Re_x}} = 2^{(3-J)/2}\frac{x}{\sqrt{\bar{\rho}\beta_s x^2/\bar{\mu}}} \approx 2^{(3-J)/2}\sqrt{\frac{\bar{\mu}}{\bar{\rho}\beta_s}} \tag{2.21}$$

As suggested by Anderson [2], these corrected quantities could be replaced by their mean or characteristic values in the boundary layer. Herein still, the characteristic values under the reference temperature are adopted, i.e., $\delta \approx 2^{(3-J)/2}\sqrt{\mu_r/\rho_r\beta_s}$. Similar to what we have done to Eq. 2.12, a simple deduction will lead to

$$\frac{\delta}{R_N} \approx 2^{1-J-\omega}\frac{\gamma^{1/4}(\gamma - 1)^{\omega/2+1/4}}{(\gamma + 1)^{1/2}}\left(1 + \frac{T_w}{T_s}\right)^{\omega/2} W_r^{1/2} \tag{2.22}$$

which shows that the SPBL thickness is proportional to the square root of W_r. Hence, the SPBL thickens slower than the shock wave as the rarefaction degree increases.

Lastly, the shock wave stand-off distance could be expressed as

$$\Delta = \Delta_{\text{inv}} + \delta^* \tag{2.23}$$

where $\Delta_{\text{inv}} = 2^{1-J}\rho_\infty a_s/(\rho_s\beta_s)$ is the stand-off distance predicted in an inviscid flow model [20], while δ^* is the displacement thickness of the SPBL resulting from the viscous effects. It is noteworthy that δ^* can be either positive or negative, due to

the dual role of the cold wall surface. On the one hand, the clod wall surface will cool the fluid near it to increase the density and thus to reduce Δ; but on the other hand, the possible real gas effects will also be frozen, leading to the increase of Δ. These dual effects are competing and may counteract each other, with the final result depending on the specific flow parameters, which itself is a topic to be studied in-depth. We will return to this problem in later discussions on the real gas effects. However, for traditional continuous flows, δ^* is relatively small and can be neglected. For hypersonic rarefied flows, the value of δ^* is generally positive, based on extension of the traditional definitions of the SPBL and the shock wave stand-off distance. Therefore, we approximately introduce herein this minor modification $\delta^* \approx 0.285\delta$, by comprehensively considering both the two-dimensional and axisymmetric flow cases. After some deductions, Eq. 2.23 can be rewritten as

$$\frac{\Delta}{R_N} \approx 2^{1-J}\left(\frac{\gamma}{2}\right)^{1/2}\frac{\gamma-1}{\gamma+1} + 0.285\frac{\delta}{R_N} \tag{2.24}$$

It seems that Δ is affected slightly by W_r.

Now, substituting Eqs. 2.20, 2.22 and 2.24 into Eq. 2.18, and considering that $\omega \approx 0.75$, $\gamma = 1.4 \sim 1.3$ and T_w/T_s is not so large, say less than 0.2, we will approximately get

$$\Theta \approx \frac{W_r + 0.9W_r^{1/2}}{0.4 + 0.26W_r^{1/2}} \tag{2.25}$$

Equation 2.25 shows a one-to-one relationship between the rarefaction criterion W_r and the flow field structure parameter Θ. Therefore, given a specific value of the single parameter W_r, the degree of flow rarefaction and the pattern of flow field structure are immediately and clearly known, which naturally confirms the rich meanings of W_r.

Figure 2.5 demonstrates the trend that Θ varies with W_r. It could be observed that $\Theta \ll 1$, as long as $W_r \ll 1$, indicating the continuum regime where both the boundary layer and shock wave are thin and in most of the region behind the shock wave, the flow could still be considered to be inviscid; as W_r increases, Θ will also increase sharply, with Θ approximately being 0.5 or 1.0 when W_r equals 0.05 or 0.2, respectively, indicating that exactly a half or the entire region behind the shock wave is dominated by the viscous flow; and $\Theta > 1$ or $\Theta \gg 1$, according to an extended meaning, corresponds to the cases where the shock wave is partly overlapped or completely merged with the boundary layer. Based on these typical flow field patterns, we can make a physical flow classification, and study the corresponding aeroheating performance in each flow regime.

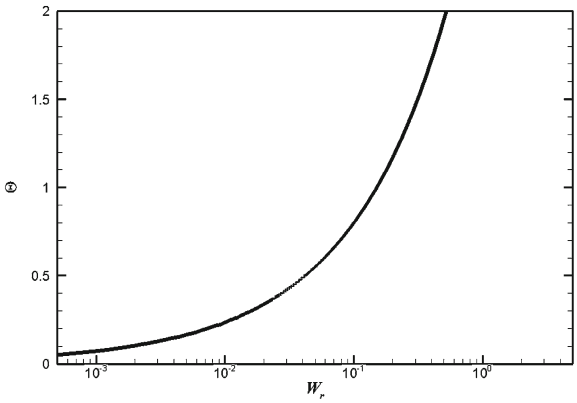


Fig. 2.5 Variation of the flow field structure parameter with the rarefaction criterion

2.3.4 Flow Regime Classification and Flow Field Structure Discussion

In the above section, it is found that as the flow transits from the continuous to the rarefied state, from the macroscopic flow field will emerge several typical patterns which indicate several stages of the rarefied gas effects from weak to strong, and thus provides a physical basis to determine the boundaries of flow regime classification. Specifically, based on the criterion W_r, hypersonic rarefied flows can be classified as follows:

(I) $W_r < 0.05$, and correspondingly, Eq. 2.25 approximately gives $\Theta < 0.5$. It means that shock wave and boundary layer are separated from each other by an inviscid region which still occupies more than half the area between the shock wave and the wall surface.

(II) $0.05 < W_r < 0.2$, and correspondingly, $0.5 < \Theta < 1.0$. Both the shock wave and the boundary layer grow, approach, and get in touch with each other ($\Theta = 1.0$) at $W_r = 0.2$, while the inviscid region gradually disappears.

(III) $0.2 < W_r < 10.0$, and $\Theta > 1.0$. In this regime, the shock wave and boundary layer overlap or even completely merge into each other. The upper limit is set according to the fact that at $W_r = 10.0$, the molecular mean free path just behind the shock wave is found to be roughly equal to the shock wave stand-off distance based on the analysis in the above subsection, i.e., $\Delta \approx \lambda_s \approx \sqrt{\pi\gamma/2}\mu_s/(\rho_s a_s)$. In this situation, molecules passing through the shock wave can directly impinge on the wall surface, which is regarded as the condition that the shock wave disappears.

(IV) $W_r > 10.0$, and $\Theta \gg 1.0$. There no longer exists shock wave or boundary layer, and the free molecular flow limit is to be approached.

In this thesis, we have also employed the DSMC method to carry a series of supporting numerical calculations. Figure 2.6 displays some typical patterns of the hyper-

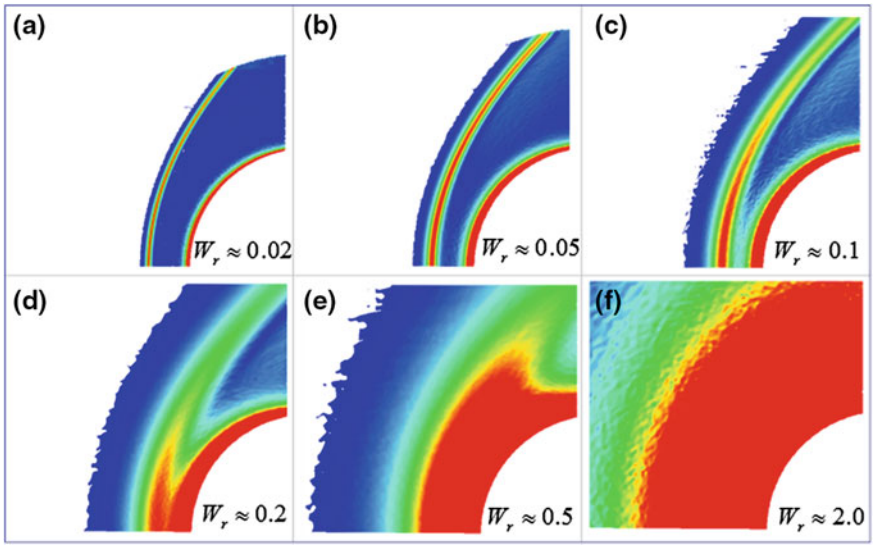


Fig. 2.6 Typical patterns of hypersonic rarefied flow field structure visualized by numerical shadowgraph

sonic rarefied flow field structure visualized by numerical shadowgraph. Although the patterns shown are two-dimensional flow cases with $M_\infty = 10$, the analysis on axisymmetric cases and other Mach numbers gives an approximately identical vision and shares the same conclusion as long as W_r is kept constant. The observed evolution characteristic of the flow field is also consistent with the above theoretical analysis, suggesting that W_r is the most important and possibly the only necessary parameter in the current problem. The corresponding scatter of microscopic molecules is shown in Fig. 2.7 which is produced using Bird's visual wind tunnel program DSMCX [21]. It also agrees with our analysis and numerical results, and the corresponding microscopic physical mechanism will be discussed in the next section.

2.3.5 Aeroheating Performance and Bridging Function

As mentioned earlier, the evolution of the flow field structure is accompanied simultaneously by the enhancement of the nonlinear factors' effects in flow and heat transfer. The several typical flow field patterns discussed in the last section are corresponded by several typical aeroheating characteristics.

In the flow regime (I), since the shock wave and boundary layer are separated far enough from each other, the viscous interaction effects or saying rarefied gas effects are negligible, and the continuous NSF equations are still valid. Quantitatively speaking, W_r represents the relative contribution of the non-Fourier heat flux terms,

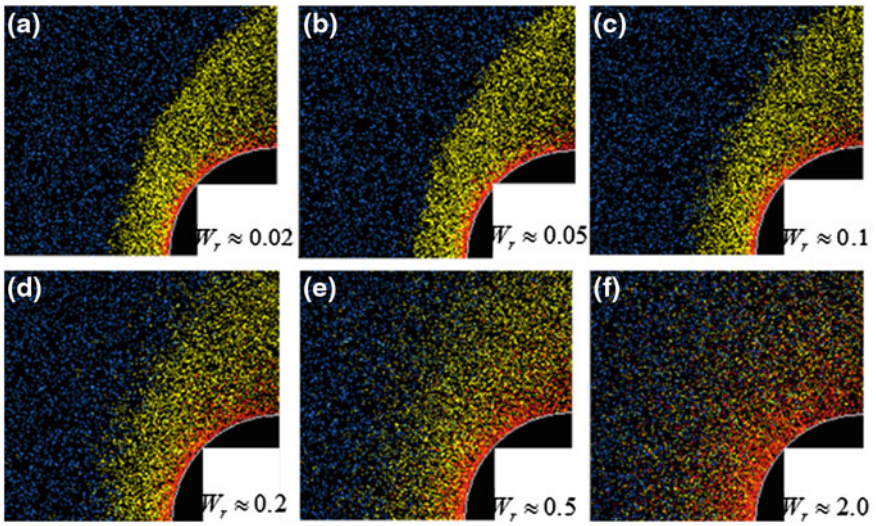


Fig. 2.7 Scatter of molecules for typical hypersonic rarefied flow fields.(The *blue dots* represent the undisturbed free stream molecules; the *red dots* represent molecules that struck the wall surface; and the *yellow dots* represent the indirectly affected molecules, i.e., those that did not strike the wall surface, but collided with the *red* "molecules" or other *yellow* ones. The *blue-yellow* transition represents the bow shock wave, while the *red-yellow* mixing represents a type of boundary layer)

and thus the relative error will be no more than 5 % when the NSF-based Fay–Riddell Eq. 2.1 is directly used to predict the stagnation point heat flux, i.e.,

$$\text{Error}\% = \frac{q_{\text{NF}}}{q_{\text{F}} + q_{\text{NF}}} = \frac{W_r}{1 + W_r} < W_r \leq 5\,\% \tag{2.26}$$

In flow regime (II), the viscous interaction effects can no longer be ignored. The shock wave and boundary layer are approaching but still do not touch each other, and so the interaction effects are not strong. Correspondingly, aeroheating is characterized by a weak nonlinear performance, and thus the non-Fourier correction terms could be directly added to the Fourier part to approximately give the actual heat flux, as shown by Eq. 2.7, or in a nondimensional form, a bridging function is obtained as

$$C_{\text{h}} = (1 + W_r) C_{\text{h,F}} \tag{2.27}$$

where the heat transfer coefficient $C_{\text{h}} = q_s/[\rho_\infty V_\infty (h_s - h_w)]$, and $C_{\text{h,F}}$ is that calculated based on Fourier's law. In practice, it is convenient to use $C_{\text{h}} = 2q_s/[\rho_\infty V_\infty^3 (1 - T_w/T_s)]$, and $C_{\text{h,F}}$ is calculated by the classical Fay–Riddell equation. The inclusion of the influence of T_w in C_{h} is significant especially for a better normalization of cases near the free molecular flow limit. Otherwise, the generally used $2q_s/(\rho_\infty V_\infty^3)$ will approach $1 - T_w/T_s$ rather than 1 if the wall surface is not

so cold. In this way, Eq. 2.27 establishes a bridge between the actual heat flux under rarefied gas effects and the prediction of the classical theory.

As $W_r > 0$, it is shown the heat flux in this regime is a little higher than the prediction of Fay–Riddell equation, which is consistent with the results [22, 23] of VSL method and higher order boundary layer method, as well as the related experimental data [9]. However, it is worth noting that if CFD method is used to numerically solve NSF equations, the heat flux will generally be overestimated. In the present theoretical modeling study, the reference standard is the analytical Fay–Riddell equation which is based on the first order boundary layer assumption without considering the viscous interaction effects, and thus underestimates the heat flux.

In fact, from a microscopic point of view, the non-Fourier heat transfer phenomenon in this regime originates from the fact that a greater proportion of molecules can directly impinge on the wall surface with less or even no collision between molecules because the MFP is larger in a rarefied (nonequilibrium or insufficient collisions) flow. While in a continuous flow (regime I), most of the molecules have to indirectly transfer part of their energy to wall surface layer-by-layer via quantities of collisions between molecules. Also as displayed by Fig. 2.7, when the flow becomes more rarefied, the concentration of the red "molecules" directly affected by the wall surface increases and their territory expands outward, while the concentration of the yellow "molecules" indirectly affected by the wall surface decreases and their territory also expands outward. These two different mechanisms result in different aeroheating performances.

In the flow regime (III), the shock wave and boundary layer have overlapped, and the interaction between them is strong. Correspondingly, a strong nonlinearity also emerges in the flow and heat transfer, and the simple formula Eq. 2.27 in regime (II) will lose its credibility. Now, it seems that we should resort to the higher order expansions of Boltzmann equation to seek for more higher order nonlinear corrections. However, it is neither feasible nor necessary, due to the fact that the higher order nonlinear terms involve even higher order differential, more complexities and uncertainties, which prohibits an analytical study. More importantly, all the models based on the continuum hypothesis, including NSF, Burnett, and the subsequent series of models, will break down if the flow rarefaction degree increases toward the free molecular flow limit. At present, prediction of aeroheating performance in this transition regime relies mainly on the empirical fitted formulas.

After re-examining the flow parameter W_r, we find that it is still able to qualitatively represent the flow rarefaction degree in this regime, although its quantitative meaning may no longer hold. Because of its good qualities, it is worth designing a simple but practical bridging function based on W_r, although lack of a strict theoretical basis like in regime (II). Actually, after comparing with our DSMC results and related experimental data, we find the following formula could capture the aeroheating performance in this regime quite accurately:

$$C_{\mathrm{h}} = \frac{W_r^{0.8}}{0.6 + W_r^{0.8}} \tag{2.28}$$

For large values of W_r, the heat transfer coefficient will approach the free molecular flow limit.

In flow regime (IV), the free molecular flow is approximately encountered, and the appropriate analysis methods include the discrete kinetic theory and the free molecular flow theory. The aeroheating performance could also be directly obtained based extendedly on Eq. 2.28.

In summary, for hypersonic rarefied flows, the aeroheating prediction methods and their scope of application are

$$C_{\mathrm{h}} = \begin{cases} C_{\mathrm{h,F}} & W_r < 0.05 \\ (1 + W_r)C_{\mathrm{h,F}} & 0.05 \le W_r \le 0.2 \\ W_r^{0.8}/(0.6 + W_r^{0.8}) & W_r \ge 0.2 \end{cases}$$

2.3.6 DSMC Results and Experimental Data

Besides the above analysis, DSMC method is used to simulate a series of cases in which $M_\infty = 5 \sim 20$, and $W_r \approx 0.02 \sim 40.0$. Figure 2.8 demonstrates a series of computed heat transfer coefficients C_{h} versus W_r, and shows their comparisons with those from Fay–Riddell equation, the bridging functions built in this thesis and DSMC results of Santos [24]. A second horizontal axis has also been given to show the corresponding Knudsen number Kn_∞ for $J = 0$, $M_\infty = 10$, $\gamma = 1.4$, and $T_w/T_s \ll 1$.

It can be observed that all the data points, including the two-dimensional and axisymmetric cases, the highly cooled and not so cold wall surface cases, our DSMC results and those from the literature [24], are normalized to fall on a single curve.

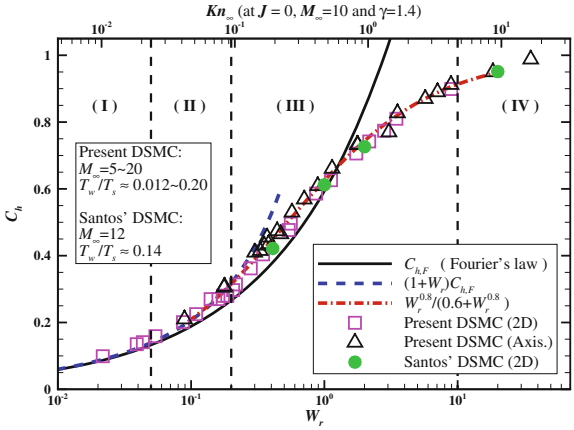


Fig. 2.8 Demonstration of the non-Fourier heat transfer and flow regime classification in hypersonic rarefied flows

This curve coincides with the one predicted by Fay–Riddell equation when $W_r \ll 1$; it departs from and becomes slightly higher than the Fay–Riddell prediction when W_r gradually increases, indicating the emergence of the weak viscous interaction or nonlinear effects. This performance is well described by Eq. 2.27; if W_r increases furthermore, the growth trend of the actual aeroheating begins to slow down, returns to Fay–Riddell prediction at $W_r \approx 1.0$, and finally tends to the free molecular flow limit. In the free molecular flow regime, almost all of the energy carried by a molecule will be transferred to the wall surface, and for a fully diffuse reflection wall surface, the heat transfer coefficient will approach 1 rather than infinity.

The comparison also shows that for a given free stream condition, an axisymmetric nose ($J = 1$) will undergo a flow of double rarefaction degree relative to the peer size two-dimensional nose ($J = 0$). In the continuous flow regime, the stagnation point heat flux of an axisymmetric nose is about 40 % higher than that of a peer size two-dimensional nose. But when the flow becomes rarefied, the difference between them reduces, and both will approach the free molecular flow limit. This indicates that the aeroheating performance of a two-dimensional nose varies more quickly with the increase in the rarefaction degree.

In addition, it is also shown by Eq. 2.25 and Fig. 2.8 that a higher surface temperature means a relative higher rarefaction degree. When the surface temperature increases, the absolute value of heat flux decreases, but the heat transfer coefficient which has already considered the influence of surface temperature actually becomes higher. From a microscopic viewpoint, this is because molecules reflected from a higher temperature wall surface have relatively higher energy and a larger MFP, and thus could penetrate further to broaden the region directly influenced by the wall surface, which is just a behavior of the rarefied flow, as also shown in Fig. 2.7.

Our research group has cooperated with the group headed by Hong-Ru Yu (academician of Chinese Academy of Sciences) at Institute of Mechanics, Chinese Academy of Sciences, and carried a series of research experiments in the shock tunnel to measure the stagnation point heat flux of several small-sized leading edge models by utilizing the coaxial thermocouple technique. The author has taken part in the design of experiment program, pre-research of the measurement principle of aeroheating on small-sized models and analysis of experimental results. In Fig. 2.9 we give two sets of measurements in the shock tunnel under stable operation. In one set, the duplicated condition is equivalent to a flight with a Mach number 6.68 at an altitude of 44 km, and the radii of curvature of spherically blunted cone models are 1 mm, 4 mm and 5 mm, respectively. In the other set, the corresponding condition is Mach number 8.7 at an altitude of 49.8 km, and radii are 1 mm, 3 mm and 5 mm, respectively. The rarefaction degree $W_r \approx 0.02 \sim 0.3$ in the experimental flows. The distribution and variation trend of the experimental data in Fig. 2.9 agree with the present analyses and DSMC results in Fig. 2.8.

In other words, both DSMC results and the experimental data validate the theoretical modeling analyses in this chapter.

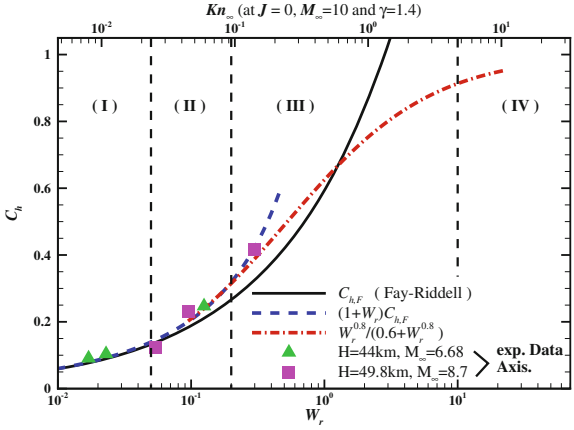


Fig. 2.9 A normalization of the shock tunnel measurements

2.3.7 Extension and Discussion of the Rarefaction Criterion

The present rarefaction criterion W_r was first introduced based on analysis of stagnation point aeroheating of sharpened noses in the near-continuum flow regime, and then its physical meanings were extended to more rarefied flows. Actually, in a broad sense, W_r represents the ratio of two characteristic timescales (the mean collisions time of molecules in the post-shock flow field to the characteristic time of local macroscopic flow), namely $W_r \sim \tau_c/\tau_f$, or ratio of two characteristic length scales (post-shock mean free path of molecules to local macroscopic flow scale), namely $W_r \sim d/R_N \sim \lambda_s/R_N \sim (\delta/R_N)^2$, as shown in the earlier discussion on the flow field structure. Therefore, W_r could be regarded as a basic characteristic flow parameter of hypersonic rarefied flows, and should apply to a boarder scope, such as the aeroheating problems downstream of the stagnation point region and the aerodynamic force-related problems.

Indeed, since W_r is derived from analysis of the nonlinear heat flux terms of Burnett equations, theoretically speaking, a similar parameter could also be derived from analysis of the corresponding nonlinear shear stress terms to characterize the non-Newton shear in hypersonic rarefied flows. In addition, as mentioned earlier, W_r is directly related to the modified Cheng's parameter K_Λ^2, and K_Λ^2 has been used to study the aerodynamic force-related problems. We have also found some researches [17] where a parameter similar to W_r is employed to normalize the drag of a flat plate in rarefied flows.

Next, to give a supporting example, we extend the physical meanings of W_r qualitatively to the downstream region of the stagnation point to show that its scope of application could be wider.

In calculating the total amount of aeroheating on TPS of the new generation vehicle, the distribution of heat flux along the downstream wall surface is also noteworthy.

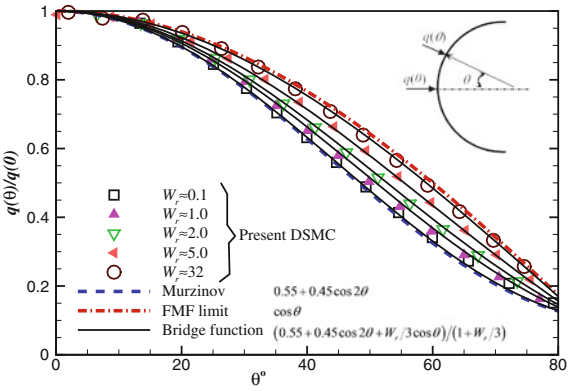


Fig. 2.10 Heat flux distributions over a spherical nose at different rarefaction degrees

However, as surveyed by the author, studies of the heat flux distribution in rarefied flows are extremely rare, and even a reliable empirical formula is unavailable. We hope to design a simple and useful formula based on W_r to estimate the evolution of the downstream heat flux distribution as the rarefication degree varies.

This extension has some physical bases. On the one hand, as the flow transits from continuous to rarefied state, the heat flux distribution undergoes a process similar to that of the stagnation point region, changing gradually from the continuous flow limit to the free molecular flow limit. In the hypersonic continuous flow regime, Murzinov [25] has given a fitted formula to describe the heat flux distribution over a spherical nose model,

$$q(\theta)/q(0) = 0.55 + 0.45\cos 2\theta \tag{2.29}$$

where θ is the angle between the free stream direction and normal direction of the surface element, as shown in Fig. 2.10. For the free molecular flows, the corresponding distribution is

$$q(\theta)/q(0) = \cos\theta \tag{2.30}$$

On the other hand, in the continuous flow regime, some theories derived in the neighborhood region of stagnation point, for instance the SPBL theory, could be extended quite far downstream. When the flow becomes rarefied, the related conclusions should be quantitatively similar. Therefore, to be concise, we introduce the following bridging function based on a weighted average.

$$\frac{q(\theta)}{q(0)} = \frac{0.55 + 0.45\cos 2\theta + (W_r/3)\cos\theta}{1 + W_r/3} \tag{2.31}$$

Figure 2.10 shows that under different flow rarefication degrees, Eq. 2.31 can predict the heat flux distribution downstream of the stagnation point with relative

accuracy. This suggests that as a characteristic flow parameter, the extended physical meanings could also be useful to describe the rarefied gas effects in the region beyond the stagnation point.

2.4 Engineering Applications

In the above section, most discussions are normalized analyses based on the nondimensional parameters. But in practical engineering applications, what is of most concern is likely to be the variation of a single dimensional parameter with the others fixed. For example, we want to know for what size of the leading edge, the rarefied gas effects will be significant at a given altitude? Or at what altitude do we have to consider the rarefied gas effects for a given leading edge? This section will make a brief discussion of these questions.

First, let us take the altitude 40 Km as a typical example. At this altitude, $T_\infty \approx 250\,\mathrm{K}$, $\rho_\infty \approx 4.0 \times 10^{-3}\,\mathrm{kg/m^3}$, $\mu_\infty \approx 1.6 \times 10^{-5}\,\mathrm{kg/(m \cdot s^2)}$, $a_\infty \approx 317\,\mathrm{m/s}$, and the MFP of molecules in the free stream $\lambda_\infty \approx 1.7 \times 10^{-5}\,\mathrm{m}$ based on the hard sphere model. Consider furthermore that a two-dimensional leading edge flies with a Mach number 10, assume the temperature of the wall surface is not so high, say for instance $T_w < 1{,}000\,\mathrm{K}$, and then we will get an engineering rarefication criterion $W_r \approx 4 \times 10^{-5}/R_N$. When $R_N > 0.8\,\mathrm{mm}$, $W_r < 0.05$, belonging to the above-mentioned flow regime (I) where Fay–Riddell equation is still valid. Not until $R_N < 0.8\,\mathrm{mm}$ does the rarefied gas effects on aeroheating become significant. But for the axisymmetric leading edge model, when $R_N = 0.8\,\mathrm{mm}$, $W_r = 0.1$, and thus Fay–Riddell equation has underestimated the heat flux by about 10 %.

At a higher altitude, the atmosphere density is lower, and then the rarefied gas effects can appear for relative larger leading edges. When the altitude increases every 16 km, the density will approximately decrease an order of magnitude. Still, considering the example of a Mach number 10 flight of a two-dimensional leading edge model, at altitude of 50 km, $W_r \approx 1.6 \times 10^{-4}/R_N$, and at altitude of 60 km, $W_r \approx 5.3 \times 10^{-4}/R_N$. The rarefaction gas effects can appear for a nose radius of 3 mm and 10 mm, respectively. And for an axisymmetric model, the corresponding radii are 6 mm and 20 mm, respectively.

However, as shown in Fig. 2.8, when $W_r < 1.0$, the actual heat flux is comparatively higher than the prediction of Fay–Riddell equation, with the maximum difference being around 20 %. Only when $W_r > 1.0$, the actual heat flux begins to be lower than the prediction of Fay–Riddell equation, which is of utmost interested in engineering practice. At an altitude of 50 km, the radii satisfying this condition should be smaller than 0.15 mm and 0.3 mm for a two-dimensional and axisymmetric leading edge model, respectively. At an altitude of 60 km, the corresponding limit radii should be 0.5 and 1.0 mm. As we see, for the 1.0 mm-sized leading edges likely to be used in engineering, not until above the altitude of 60 km, does Fay–Riddell equation begin to underestimate the stagnation point heat flux.

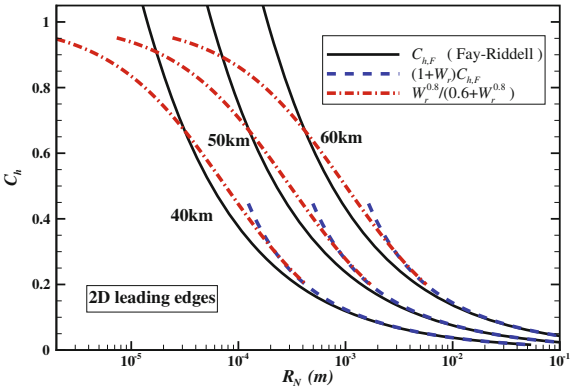


Fig. 2.11 The stagnation point heat transfer coefficient of a two-dimensional leading edge varies with noses' radi

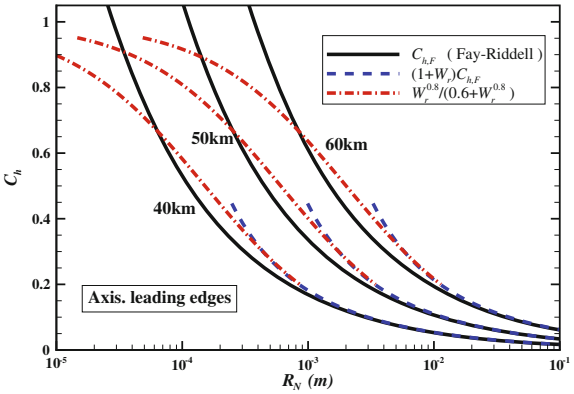


Fig. 2.12 The stagnation point heat transfer coefficient of an axisymmetric leading edge varies with noses' radii

Figures 2.11 and 2.12 demonstrate variations of the stagnation point heat transfer coefficient for a two-dimensional and an axisymmetric leading edge model, respectively, as the noses' radii decrease at three altitudes. Comparison between the bridging functions and Fay–Riddell prediction shows the rarefied gas effects on aeroheating performance.

2.5 Chapter Summary

In this chapter, the theoretical modeling method has been used to study the rarefied gas effects resulting from microscopic insufficient collisions of molecules and their influence on the aeroheating performance of sharpened leading edges.

First, we propose a physical model at the stagnation point region of a slightly blunted nose in the near-continuum flow regime, in order to analyze the macroscopic performance of rarefied gas effects, i.e., the gradual enhancement of effects of nonlinear factors in the flow and heat transfer. The ratio of the nonlinear non-Fourier to the linear Fourier heat flux terms is defined as a characteristic flow parameter W_r to represent the relative impact of the nonlinear factors and to indicate the failure of NSF equations. A further extension analysis showed that W_r measures the strength of the rarefied gas effects in the whole flow regime, and could be regarded as a general rarefication criterion with physical meanings for aeroheating-related problems.

Secondly, it was found that the rarefication criterion W_r could also be useful to predict the evolution of the flow field structure features as the rarefication degree of the flow varies. A regime classification of hypersonic rarefied flows was made based on a detailed analysis of several typical patterns of the flow field structure. In each flow regime, the aeroheating performance and the corresponding microscopic physical mechanism were discussed. According to the physical meanings of W_r and the subsequent extension, bridging functions were established, for the purpose of engineering applications, to fast predict the stagnation point heat flux and the distribution of the downstream heat flux.

Lastly, the reasonability of the present theoretical analysis and reliability of the bridging functions were validated through various comparisons with supporting DSMC calculations and experimental measurements. In addition, applications of the rarefication criterion in the engineering practice were also discussed.

References

1. Fay JA, Riddell FR (1958) Theory of stagnation point heat transfer in dissociated air. J Aeronaut Sci 25(2):73–85
2. Anderson JD (2006) Hypersonic and high temperature gas dynamics, 2nd edn. AIAA Inc, Reston
3. Chapman S, Cowling TG (1970) The mathematical theory of non-uniform gases, 3rd edn. Cambridge University Press, Cambridge
4. Tsien H-S (1948) Engineering and engineering sciences. J Chin Inst Eng 6:1–14
5. Lockerby DA, Reese JM, Struchtrup H (2009) Switching criteria for hybrid rarefied gas flow solvers. Proc R Soc A 465:1581–1598
6. Matting FW (1964) General solution of the laminar compressible boundary layer in the stagnation region of blunt bodies in axisymmetric flow. NASA Technical Note, D-2234
7. Macrossan MN (2006) Scaling parameters for hypersonic flow: correlation of sphere drag data. In: 25th international symposium rarefied gas dynamics, pp 759–764
8. Cheng HK (1963) The blunt-body problem in hypersonic flow at low Reynolds number. Technical report, Cornell Aeronautical Laboratory
9. Engel CD, Praharaj SC (1983) Minnver upgrade for the AVID system. NASA Contractor Report 172212:126 (volume 1: Lanmin user's manual)
10. Waldron HF (1967) Viscous hypersonic flow over pointed cones at low Reynolds numbers. AIAA J 5(2):208–218
11. Nomura S (1982) Correlation of hypersonic stagnation point heat transfer at low Reynolds numbers. AIAA J 21(11):1598–1600

12. Artamonov AK, Arkhipov VN, Farafonov VG (1981) Dimensionless numbers in the aerodynamics of low-density gases. Fluid Dyn 16(1):110–114
13. Gupta RN, Simmonds AL (1986) Hypersonic low-density solutions of the Navier-Stokes equations with chemical nonequilibrium and multicomponent surface slip. AIAA Paper, pp 1986–1349
14. Gupta Roop N, Jones Jim J, Rochelle William C (1992) Stagnation-point heat-transfer rate predictions at aeroassist flight conditions. Nasa Technical Paper 3208:19
15. Wittliff CF, Wilson MR (1961) Low-density stagnation-point heat transfer in hypersonic air flow. Technical report. Aeronautical Research Laboratory, Air Force Research Division, Air Research and Development Command, United States Air Force
16. Riabov VV (2006) Numerical simulation of kinetic effects in low-density hypersonic aerodynamics. Rivier Acad J 2(2):17
17. Fan J, Wu C-X, Sun Q-H, Jiang J-Z (2009) Kinetic analysis of the flow past a flat plate at moderate Reynolds numbers. Adv Mech 39:421–425
18. Robben F, Talbot L (1966) Measurements of shock wave thickness by the electron beam fluorescence method. Phys Fluids 9:633
19. Macrossan MN, Lilley CR (2003) Viscosity of argon at temperatures >2000 K from measured shock thickness. Phys Fluids 15:3452
20. Wen CY, Hornung HG (1995) Non-equilibrium dissociating flow over spheres. J Fluid Mech 299(1):389–405
21. Bird GA (1994) Molecular gas dynamics and the direct simulation of gas flows. Oxford University Press, Oxford
22. Kolodziej P (1997) Aerothermal performance constraints for hypervelocity small radius unswept leading edges and nosetips. Nasa Technical Memorandum, 112204
23. Kao HC (1964) Hypersonic viscous flow near the stagnation streamline of a blunt body: II. third-order boundary-layer theory and comparison with other methods. AIAA J 2(11):1898–1906
24. Santos WFN, Lewis MJ (2003) Aerodynamic heating performance of power law leading edges in rarefied hypersonic flow. AIAA Paper, pp 2003–3894
25. Murzinov IN (1966) Laminar boundary layer on a sphere in hypersonic flow of equilibrium dissociating air. Fluid Dynam 1(2):131–133

Springer

http://www.springer.com/978-3-662-44364-4

Theoretical Modelling of Aeroheating on Sharpened Noses Under Rarefied Gas Effects and Nonequilibrium Real Gas Effects

Wang, Z.-H.

2015, XV, 94 p. 46 illus., 27 illus. in color., Hardcover
ISBN: 978-3-662-44364-4